

Elasto-dynamic analysis of a novel 2-DoF rotational parallel mechanism with an articulated travelling platform

Yimin Song · Gang Dong · Tao Sun · Binbin Lian

Received: 25 September 2014 / Accepted: 28 December 2014 / Published online: 27 January 2015
© Springer Science+Business Media Dordrecht 2015

Abstract This paper carries out the elasto-dynamic analysis of a novel 2 degrees-of-freedom (DoF) rotational parallel mechanism (RPM) with an articulated travelling platform by means of kineto-elasto dynamic method. The architecture of the proposed 2-DoF RPM is firstly described, and then its kinematic analysis is carried out by closed-loop vector method. On the basis of finite element analysis, the elasto-dynamic models of movable components are established before assembling to formulate the elasto-dynamic equations of the whole mechanism in the light of deformation compatibility conditions. The free vibration equation is then achieved to evaluate the natural frequency of the novel 2-DoF RPM. Finally, an example is illustrated and the results are verified by finite element software. It shows that the relatively high natural frequencies and good dynamic performance make the novel 2-DoF RPM a promising solution for pose-adjusting module of 5-DoF machine centre.

Keywords Rotational parallel mechanism · Elasto-dynamics · Finite element analysis · Natural frequency

1 Introduction

With the increasing demand for orientation capacity in the machining of aerospace components with large size, thin wall and complex surface, 5 degree-of-freedom (DoF) hybrid mechanisms consisting of 3-DoF parallel mechanism and 2-DoF pose-adjusting mechanism have been accepted as an effective substitution of the traditional serial NC machines [1], in terms of higher dynamic performance, better accuracy and larger load-weight ratio. The famous Tricept mechanism [2–6] is a successful example of 5-DoF hybrid mechanism who wisely combines the advantages of parallel and serial mechanisms. However, it should be pointed out that the 2-DoF pose-adjusting module attached to Tricept mechanism is open-loop serial structure, and it would be designed inevitably towards large scale and huge weight in order to meet the requirements of high stiffness of the whole mechanism, which makes it a major obstacle to application. With the merit of good rigidity and compact structure, 2-DoF rotational parallel mechanism (RPM) is superior to the serial counterpart as an integration of 5-DoF hybrid mechanism.

As far as 2-DoF RPM is concerned, extensive researches [7–15] have been carried out over the decades. Spherical 5R mechanism is the earliest and simplest parallel mechanism to achieve the two rotational DoFs, whose kinematics was thoroughly discussed by Kong and Liu [7–9]. Herein, R denotes the revolute joint. By introducing parallelogram

Y. Song · G. Dong · T. Sun (✉) · B. Lian
Key Laboratory of Mechanism Theory and Equipment
Design Ministry of Education, Tianjin University,
Tianjin 300072, China
e-mail: stao@tju.edu.cn

linkage to the mechanism, Baumann [10] proposed a 2-DoF RPM named PantoScope and applied it to the micro-invasive surgery. In order to deal with large orientation workspace problem of the laser detection in aerospace, Ross–Hime Designs [12] developed the famous Omni-Wrist III, whose kinematics is investigated by Sofka [13] while the rigid dynamics is analyzed by Chen [14]. It is believed that Omni-Wrist III has the advantage of good rotational capacities without singularity. In addition, several decoupled 2-DoF RPM are proposed by Liu [15].

It is found out that kinematic capacities are the main concern of the above-mentioned 2-DoF RPMs. However, it comes to the application for pose-adjusting module of 5-DoF machine center, stiffness and elastic dynamic performance need to be taken into account, which might be the shortcomings of some 2-DoF RPMs above.

Driven by the demands for pose-adjusting module with high stiffness and good dynamic performance in machining aerospace components, a novel 2-DoF RPM [16] with an articulated travelling platform is proposed and its elasto-dynamic analysis is investigated in this paper. The proposed 2-DoF RPM is believed to be without parasitic motion, good rotational capability and can be designed potentially as a compact module with large ratio of stiffness to weight. The organization of the paper is as follows: after introducing the underlying architecture of the proposed 2-DoF RPM in Sects. 2, 3 carries out the inverse kinematics by closed-loop vector method. In Sect. 4, the elasto-dynamic modeling of components is formulated and that of the whole mechanism is achieved. The natural frequencies of the 2-DoF RPM are then analyzed through an example and verified by the finite element software in Sect. 5. Finally, conclusions are drawn in Sect. 6.

2 Underlying architecture

As shown in Fig. 1, the novel 2-DoF RPM is composed of a fixed base, an articulated travelling platform and two parallelogram-based limbs. The articulated travelling platform includes sub-plate I and sub-plate II, which are articulated to each other by one R joint, in which sub-plate I is regarded as the output link that connects rigidly to the end-effector. Each parallelogram-based limb contains one actuated component (represented by A or B) and two identical

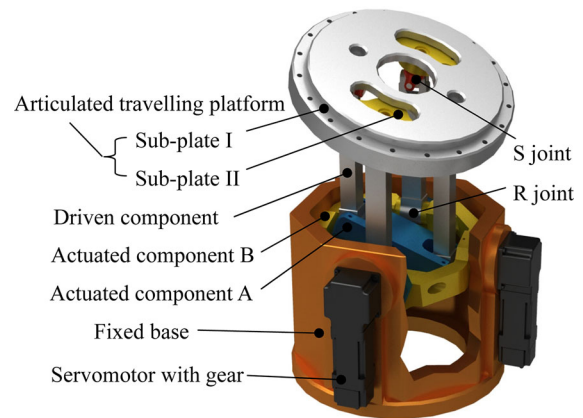


Fig. 1 Conceptual design of the novel 2-DoF RPM with an articulated travelling platform

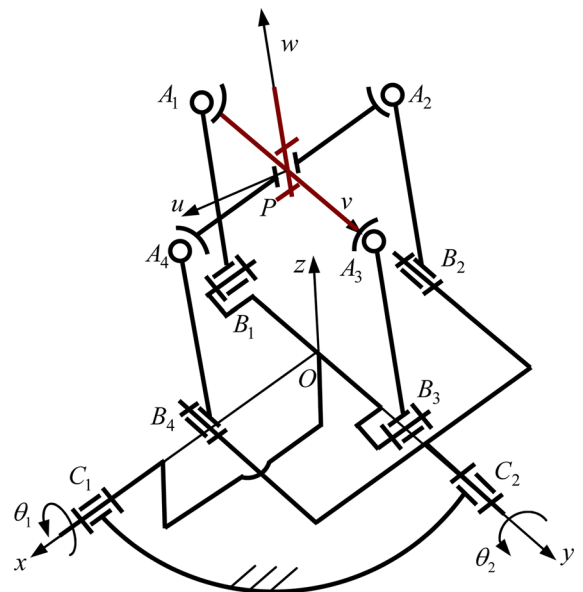


Fig. 2 Schematic diagram of the novel parallel mechanism

driven components. The actuated component A or B is adjacent to the fixed base by R joint. And the driven component connects to the actuated component and sub-plate by R joint and S joint, respectively. Herein, S represents spherical joint.

As is shown Fig. 2, A_i and B_i ($i = 1-4$) denote the centers of the i th S joint and the i th R joint in the actuated components. O denotes the intersection point of B_1B_3 and B_2B_4 , P represents the center of the articulated R joint, and C_j ($j = 1, 2$) is the center of the R joint in actuated component (A or B). The axes of the R joints at C_1 , B_1 , and B_3 are parallel to each other, and

parallel axes also exist in R joints at C_2, B_2 and B_4 . The axes of R joints in actuated component A and those in actuated component B are perpendicular. It is noticed that the axis of articulated R joint is normal to the plane of sub-plate I. Moreover, the lengths of the driven components are all equal to l_{ab} .

In what follows, the two rotations produced by the novel parallel mechanism will be described. As shown in Fig. 2, $A_1A_3B_3B_1$ and $A_2A_4B_4B_2$ are two parallelograms, and the point P is a fixed point on the z axis due to the constraint of the revolute joints at B_i . As a result, the pose of B_1B_3 can be determined by actuating the revolute joint at C_1 with θ_1 , and then A_1A_3 can rotate about the x axis with θ_1 . Similarly, the pose of B_2B_4 can be determined by actuating the revolute joint at C_2 with θ_2 , which leads that A_2A_4 can rotate about the y axis with θ_2 , and then A_1A_3 can rotate about the v axis. Therefore, the novel parallel mechanism has two DoFs actuated by the revolute joints at C_1 and C_2 .

For the sake of describing the motion of the proposed 2-DoF RPM, several coordinate systems are established as follows. As shown in Fig. 2, a fixed coordinate system designated as $O - xyz$ is fixed at point O with the x and y axis pointing to point C_1 and C_2 , respectively. A moving coordinate system $P - uvw$ is assigned to point P with the v axis pointing to point A_3 and the w axis perpendicular to the sub-plate I. Then the orientation matrix \mathbf{R} of the frame $P - uvw$ with respect to the frame $O - xyz$ can be expressed as

$$\begin{aligned} \mathbf{R} &= \mathbf{R}_z \mathbf{R}_\beta = \begin{bmatrix} 1 & 0 & 0 \\ 0 & c\alpha & -s\alpha \\ 0 & s\alpha & c\alpha \end{bmatrix} \begin{bmatrix} c\beta & 0 & s\beta \\ 0 & 1 & 0 \\ -s\beta & 0 & c\beta \end{bmatrix} \\ &= \begin{bmatrix} c\beta & 0 & s\beta \\ s\alpha s\beta & c\alpha & -s\alpha c\beta \\ -c\alpha s\beta & s\alpha & c\alpha c\beta \end{bmatrix} = [\mathbf{u} \quad \mathbf{v} \quad \mathbf{w}] \end{aligned} \tag{1}$$

where c and s denote cosine and sine, respectively; α and β represent the angles about the x and the v axis, respectively; $\mathbf{u}, \mathbf{v}, \mathbf{w}$ denote the unit vectors of the u, v, w axes in the coordinate system $O - xyz$, respectively.

3 Kinematic analysis

After the architecture of the novel 2-DoF RPM is outlined in Sect. 2, it is necessary to carry out the

kinematic analysis including inverse position, velocity and acceleration before formulating elastic-dynamic model of mechanism.

3.1 Constraint equations

As shown in Fig. 2, the closed-loop vector equation of the novel 2-DoF RPM can be expressed as

$$\mathbf{r} = \mathbf{b}_i + l_{ab}\mathbf{w}_i - \mathbf{R}\mathbf{a}_{0i} \tag{2}$$

where $\mathbf{r} = [x_p \quad y_p \quad z_p]^T$ and \mathbf{b}_i denote the position vectors of point P and B_i in the coordinate system $O - xyz$, respectively. \mathbf{a}_{0i} represents the position vector of point A_i in the coordinate system $P - uvw$. \mathbf{w}_i represents the unit vector of A_iB_i ($i = 1-4$), and $\mathbf{a}_{01} = -\mathbf{a}_{03} = r_1[0 \quad -1 \quad 0]^T$. In addition

$$\begin{aligned} \mathbf{b}_1 &= -\mathbf{b}_3 = r_1[0 \quad -c\theta_1 \quad -s\theta_1]^T \\ \mathbf{b}_2 &= -\mathbf{b}_4 = r_2[-c\theta_2 \quad 0 \quad s\theta_2]^T \end{aligned}$$

Herein, r_1 and r_2 denote the lengths of PA_1 and PA_2 , respectively.

The driven components A_2B_2 and A_4B_4 are constrained by the R joints of the same parallelogram-based link to move within the plane $y = 0$. By taking dot product with $\mathbf{e}_y = [0 \quad 1 \quad 0]^T$ on both sides of Eq. (2) when $i = 2, 4$, the constraint equation is yielded as follows

$$y_p = 0 \tag{3}$$

Similarly, the driven components A_1B_1 and A_3B_3 are constrained by the R joints of the same parallelogram-based link to move within the plane $x = 0$, which yields

$$x_p = 0 \tag{4}$$

Furthermore, \mathbf{w}_i ($i = 1-4$) is parallel to \mathbf{r} . Hence, $\mathbf{w}_i = [0 \quad 0 \quad 1]^T$ and

$$z_p = l_{ab} \tag{5}$$

3.2 Inverse position analysis

The input parameters are represented by θ_1 and θ_2 , which are the rotational angles about x and y -axis. Substitute Eq. (3)–(5) into Eq. (2) when $i = 1$ and $i = 2$, respectively, yields $\mathbf{R}\mathbf{a}_{02} = \mathbf{b}_2$, and

$$\theta_1 = \alpha \tag{6}$$

$$\begin{aligned} \mathbf{w} &= \frac{\mathbf{Ra}_{02} \times \mathbf{v}}{\|\mathbf{Ra}_{02} \times \mathbf{v}\|} \\ &= \frac{1}{\sqrt{1 - s^2\theta_1 s^2\theta_2}} [c\theta_1 s\theta_2 \quad -s\theta_1 c\theta_2 \quad c\theta_1 c\theta_2]^T \end{aligned} \quad (7)$$

Noticing that $\mathbf{w} = [s\beta \quad -s\alpha c\beta \quad c\alpha c\beta]^T$, θ_2 can be calculated as

$$\theta_2 = \arctan\left(\frac{\tan \beta}{\cos \alpha}\right) \quad (8)$$

3.3 Velocity analysis

Taking the derivatives of Eq. (2) with respect to time yields

$$\dot{\theta}_1 \mathbf{e}_x \times \mathbf{b}_1 - \boldsymbol{\omega} \times \mathbf{Ra}_{01} = 0 \quad (9)$$

$$\dot{\theta}_2 \mathbf{e}_y \times \mathbf{b}_2 - (\boldsymbol{\omega} - \dot{\theta} \mathbf{w}) \times \mathbf{Ra}_{02} = 0 \quad (10)$$

where $\boldsymbol{\omega}$ represents the angular velocity of the sub-plate I, $\dot{\theta}$ denotes the angular velocity of the sub-plate II with respect to the sub-plate I, and $\dot{\theta}_1, \dot{\theta}_2$ are the angular velocities of the actuated component A and B.

Taking dot product with \mathbf{e}_y and \mathbf{w} on both sides of Eq. (9) and Eq. (10), yields

$$\dot{\theta}_1 = \mathbf{e}_x^T \boldsymbol{\omega} \quad (11)$$

$$\dot{\theta}_2 = \frac{(\mathbf{Ra}_{02} \times \mathbf{w})^T}{\mathbf{e}_y^T (\mathbf{b}_2 \times \mathbf{w})} \boldsymbol{\omega} \quad (12)$$

Rewriting Eq. (11) and (12) in matrix form as

$$\begin{bmatrix} \dot{\theta}_1 \\ \dot{\theta}_2 \end{bmatrix} = \begin{bmatrix} \mathbf{e}_x^T \\ \frac{(\mathbf{Ra}_{02} \times \mathbf{w})^T}{\mathbf{e}_y^T (\mathbf{b}_2 \times \mathbf{w})} \end{bmatrix} \boldsymbol{\omega} = \mathbf{J} \boldsymbol{\omega} \quad (13)$$

where \mathbf{J} is the Jacobian matrix that represents the mapping relationships between the joint velocity and the operated velocity.

3.4 Acceleration analysis

Taking the derivatives of Eq. (9) and Eq. (10) with respect to time yields

$$\ddot{\theta}_1 = \mathbf{e}_x^T \boldsymbol{\varepsilon} \quad (14)$$

$$\ddot{\theta}_2 = \frac{(\mathbf{Ra}_{02} \times \mathbf{w})^T}{\mathbf{e}_y^T (\mathbf{b}_2 \times \mathbf{w})} \boldsymbol{\varepsilon} + \mathbf{f} \boldsymbol{\omega} \quad (15)$$

where $\boldsymbol{\varepsilon}$ presents the angular acceleration of the sub-plate I, $\ddot{\theta}_1, \ddot{\theta}_2$ denotes the angular acceleration of the actuated component A and B, respectively. And

$$\mathbf{f} = \begin{bmatrix} \dot{\theta}_1 \frac{s\theta_2 c\theta_2}{c^2\theta_1} + \dot{\theta}_2 (c^2\theta_2 - s^2\theta_2) \tan \theta_1 \\ 0 \\ \dot{\theta}_1 \frac{c^2\theta_2}{c^2\theta_1} - 2\dot{\theta}_2 \tan \theta_1 c\theta_2 s\theta_2 \end{bmatrix}^T$$

4 Elasto-dynamic modeling

In the light of kineto-elasto dynamic (KED) method, the elasto-dynamic modeling of the novel 2-DoF RPM is established on the basis of inverse kinematic analysis. The elastic-dynamic model of components (actuated component, driven component and articulated travelling platform) need to be firstly considered before formulating the elastic-dynamic equation of the whole mechanism by deformation compatibility condition.

Considering the geometry of the mechanism and the requirements of KED method, several assumptions are made as follows:

- (1) Fixed base and articulated travelling platform are regarded as rigid bodies due to their relatively high rigidity, while the other components are treated as the Euler–Bernoulli spatial beams. Frictions among contact surface are negligible.
- (2) Deformations of components satisfy linear superposition principle. The transverse displacements of the spatial beam follow the cubic polynomial distribution and the longitudinal ones follow the linear distribution.
- (3) Orientation matrixes remain constant during the coordinate transformations according to the instantaneous structure hypothesis.

Some basic theory of KED method [17] is set forth as follow. In order to deal with component elastic-dynamic problem, element coordinate system $E_i - \bar{x}\bar{y}\bar{z}$ is established as shown in Fig. 3. Elastic deformation $\boldsymbol{\delta}_j$ of any point on spatial beam element can be described as

$$\boldsymbol{\delta}_j = \mathbf{N} \mathbf{u}, \quad \dot{\boldsymbol{\delta}}_j = \mathbf{N} \dot{\mathbf{u}}$$

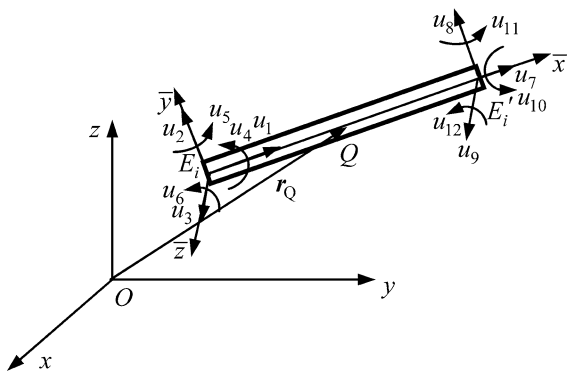


Fig. 3 The spatial beam element

where \mathbf{u} denotes the generalized coordinate vector of the element in the coordinate system $E_i - \bar{x}\bar{y}\bar{z}$ and $\mathbf{u} = [u_1 \ u_2 \ \dots \ u_{12}]^T$, \mathbf{N} represents the type-function matrix [18].

Therefore, the kinetic energy equation of the spatial beam element are formulated as

$$T = \frac{1}{2} \int_0^l \rho A_c \dot{\mathbf{u}}^T \dot{\mathbf{u}} d\bar{x} \tag{16}$$

where ρ , A_c , l represent the density, cross section area and the length of the element.

Then the potential energy equation of the spatial beam element can be formulated

$$U = \frac{1}{2} \int_0^l [EA_c (U')^2 + EI_{\bar{z}} (V'')^2 + EI_{\bar{y}} (W'')^2 + GJ (\theta')^2] d\bar{x} - \int_0^l \rho A_c \mathbf{g}^T \mathbf{r}_Q d\bar{x} \tag{17}$$

where E , I_y , I_z represent the Young's modulus, flexural section modulus of the element. U' , θ' denote the first derivation of the longitudinal displacements of any point Q in the element with axis \bar{x} . V'' , W'' denote the second derivation of the transverse displacements of point Q with axes \bar{y} and \bar{z} , respectively. \mathbf{g} is the acceleration vector of gravity. \mathbf{r}_Q denotes the position vector of Q in the coordinate system $E_i - \bar{x}\bar{y}\bar{z}$.

The motion differential equation of the spatial beam element can be formulated based on the Lagrange equation.

$$m\ddot{\mathbf{u}} + \mathbf{k}\mathbf{u} = \mathbf{f} + \mathbf{q} \tag{18}$$

where \mathbf{m} , \mathbf{k} , \mathbf{f} and \mathbf{q} represent mass matrix, stiffness matrix, interactive force vector and external force vector in the coordinate system $E_i - \bar{x}\bar{y}\bar{z}$.

When calculated in the fixed coordinate system $O - xyz$, Eq. (18) can be rewritten as

$$M\ddot{\mathbf{U}} + \mathbf{K}\mathbf{U} = \mathbf{F} + \mathbf{Q} \tag{19}$$

where $M = T^T m T$, $K = T^T k T$, $F = T^T f$, $Q = T^T q$, $T = \text{diag}(R_e^T \ R_e^T \ R_e^T \ R_e^T)$, R_e is the transformation matrix of the coordinate system $E_i - \bar{x}\bar{y}\bar{z}$ with respect to the frame $O - xyz$.

4.1 Elasto-dynamic modeling of components

4.1.1 The actuated component A

Considering the geometry of the actuated component A, 7 elastic-elements connected by 8 nodes are applied to describe the elastic-dynamic model as shown in Fig. 4. The corresponding coordinate system of each element is then established.

The boundary condition of actuated component A is analyzed. Node 11 of actuated component A coincides with point C_1 of the fixed base, resulting in the elastic deformations of Node 11 becoming 0 according to the instantaneous structure hypothesis. Affected by R joint, elastic angle about \bar{y}_{A4} -axis of Node 15 is released and the other deformations are 0. Hence the generalized coordinate vector \mathbf{U}_1 of component A can be written as $\mathbf{U}_1 = [U_{A1} \ U_{A2} \ \dots \ U_{A37}]^T$ in the fixed coordinate system $O - xyz$. Herein, $U_{A1} \sim U_{A18}$, $U_{A20} \sim U_{A37}$ represent the elastic deformations of Node 12–14, Node 16–18 in sequence, and U_{A19} denotes the elastic angle of Node 15. Then the differential motion equation of the actuated component A can be formulated as follows.

$$M_1 \ddot{\mathbf{U}}_1 + K_1 \mathbf{U}_1 = \mathbf{F}_1 + \mathbf{Q}_1 \tag{20}$$

where M_1 , K_1 , F_1 , Q_1 represent the mass matrix, the stiffness matrix, the interactive force vector and the external force vector of the actuated component A in the coordinate system $O - xyz$. Herein,

$$M_1 = \sum_{i=1}^7 J_{Ai}^T M_{Ai} J_{Ai}, \quad K_1 = \sum_{i=1}^7 J_{Ai}^T K_{Ai} J_{Ai}$$

$$F_1 = \sum_{i=1}^7 J_{Ai}^T F_{Ai}, \quad Q_1 = \sum_{i=1}^7 J_{Ai}^T Q_{Ai}$$

where M_{Ai} , K_{Ai} , F_{Ai} , Q_{Ai} denote the mass matrix, the stiffness matrix, the interactive force vector and the external force vector of the element in the

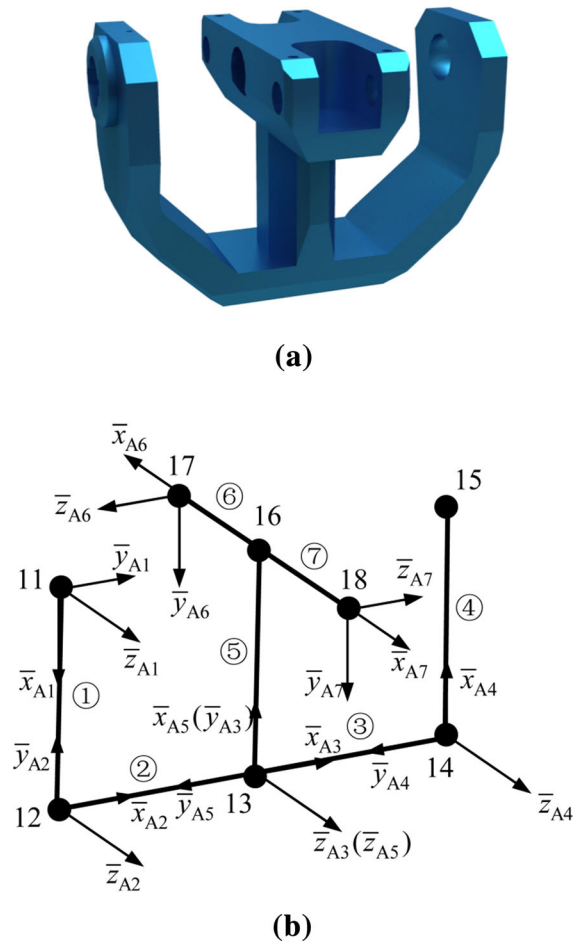


Fig. 4 The model of actuated component A. **a** The virtual prototype. **b** The finite element model

coordinate system $O - xyz$. J_{Ai} is the mapping matrix between the generalized coordinate vector of the element i and U_1 .

4.1.2 The actuated component B

As shown in Fig. 5, the actuated component B can be divided into eight elastic-elements with eight nodes. And the coordinate system of each element is established.

Similar to component A, boundary conditions of actuated component B need to be considered. Node 21 is in correspondence with point C_2 of the fixed base, and Node 25 is influenced by R joint. The generalized coordinate vector U_2 of component B can be written as $U_2 = [U_{B1} \ U_{B2} \ \dots \ U_{B37}]^T$ in

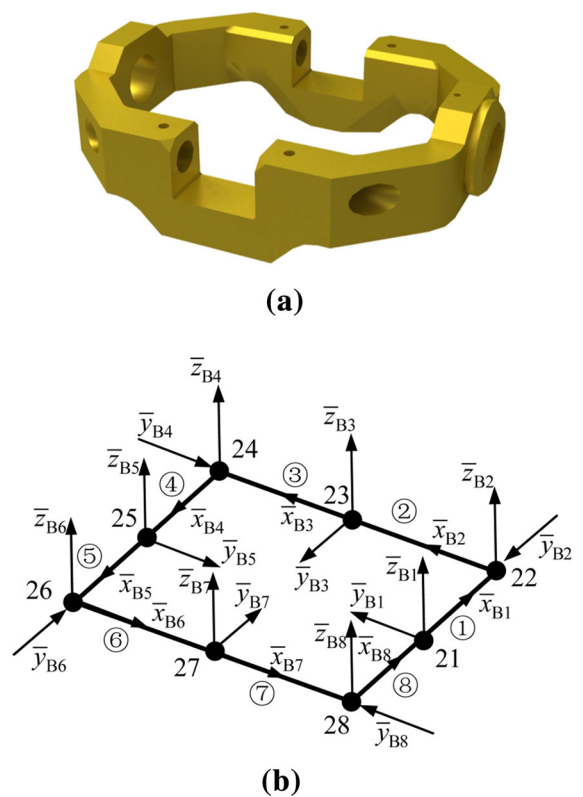


Fig. 5 The model of actuated component B. **a** The virtual prototype. **b** The finite element model

the fixed coordinate system $O - xyz$. Herein, $U_{B1} \sim U_{B18}$, $U_{B20} \sim U_{B37}$ represent the elastic deformations of Node 22–24, Node 26–28 in sequence, and U_{B19} denotes the elastic angle of Node 25. Then the differential motion equation of the actuated component B can be derived as follows.

$$M_2 \ddot{U}_2 + K_2 U_2 = F_2 + Q_2 \tag{21}$$

where M_2 , K_2 , F_2 , Q_2 represent the mass matrix, the stiffness matrix, the interactive force vector and the external force vector of the actuated component B in the frame $O - xyz$. Herein,

$$M_2 = \sum_{i=1}^8 J_{Bi}^T M_{Bi} J_{Bi}, \quad K_2 = \sum_{i=1}^8 J_{Bi}^T K_{Bi} J_{Bi}$$

$$F_2 = \sum_{i=1}^8 J_{Bi}^T F_{Bi}, \quad Q_2 = \sum_{i=1}^8 J_{Bi}^T Q_{Bi}$$

where M_{Bi} , K_{Bi} , F_{Bi} , Q_{Bi} represent the mass matrix, the stiffness matrix, the interactive force vector and the external force vector of the element in the

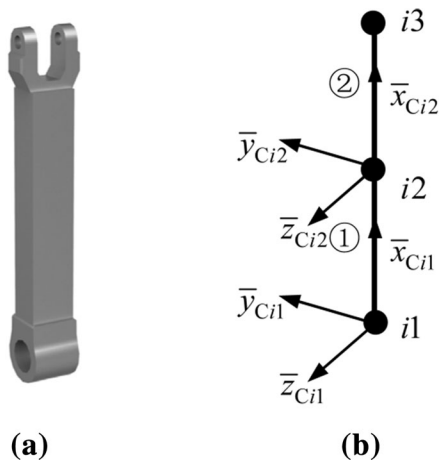


Fig. 6 The model of the driven component. **a** The virtual prototype. **b** The finite model

coordinate system $O - xyz$. J_{Bi} is the mapping matrix between the generalized coordinate vector of the element i and U_2 .

4.1.3 The driven component

The driven component is with simple structure, thus can be divided into two elastic-elements with three nodes as shown in Fig. 6. And the coordinate systems of the two elements are parallel to each other.

The generalized coordinate vector U_{2+i} of the i th ($i = 1-4$) driven component in the fixed coordinate system $O - xyz$ can be written as $U_{2+i} = [U_{Ci1} \ U_{Ci2} \ \dots \ U_{Ci18}]^T$. Herein, $U_{Ci1} \sim U_{Ci18}$ represent the elastic deformations of Node $i1-i3$ in sequence. Thus the differential motion equation of the driven component can be written as follows.

$$M_{2+i}\ddot{U}_{2+i} + K_{2+i}U_{2+i} = F_{2+i} + Q_{2+i}, \quad (i = 1 \sim 4) \tag{22}$$

where M_{2+i} , K_{2+i} , F_{2+i} , Q_{2+i} denote the mass matrix, the stiffness matrix, the interactive force vector and the external force vector of the i th driven component in the coordinate system $O - xyz$. Herein,

$$M_{2+i} = \sum_{j=1}^3 J_{Cij}^T M_{Cij} J_{Cij}, \quad K_{2+i} = \sum_{j=1}^3 J_{Cij}^T K_{Cij} J_{Cij}$$

$$F_{2+i} = \sum_{j=1}^3 J_{Cij}^T F_{Cij}, \quad Q_{2+i} = \sum_{j=1}^3 J_{Cij}^T Q_{Cij}$$

Table 1 The parameters of the virtual prototype

Parameter	Value
Density $\rho/\text{kg m}^{-3}$	7,800
Young's modulus E/Pa	2.06×10^{11}
Shear modulus G/Pa	7.94×10^{11}
Actuated component A (length/width/height)/m	
Element 1/4	0.105/0.014/0.07
Element 2/3	0.08/0.023/0.055
Element 5	0.015/0.036/0.07
Element 6/7	0.06/0.047/0.06
Actuated component B (length/width/height)/m	
Element 1/4/5/8	0.0625/0.015/0.033
Element 2/3/5/6	0.086/0.025/0.033
Element of driven component (length/width/height)/m	
	0.08375/0.019/0.026
Sub-plate I	
Mass/kg	5.4
$I_u/\text{kg m}^2$	0.04
$I_v/\text{kg m}^2$	0.04
$I_w/\text{kg m}^2$	0.06
Sub-plate II	
Mass/kg	3.27
$I_u/\text{kg m}^2$	0.01
$I_v/\text{kg m}^2$	0.01
$I_w/\text{kg m}^2$	0.03

where M_{Cij} , K_{Cij} , F_{Cij} , Q_{Cij} represent the mass matrix, the stiffness matrix, the interactive force vector and the external force vector of the element in the coordinate system $O - xyz$. J_{Cij} is the mapping matrix between the generalized coordinate vector of the element j and U_{2+i} .

4.1.4 The articulated travelling platform

Although the articulated travelling platform is assumed to be rigid component, its displacement would be affected by the deformation of the elastic components. Therefore, the dynamic equations of the articulated travelling platform are formulated in the fixed coordinate system $O - xyz$ as

$$M_{Pi}\ddot{U}_{Pi} = F_{Pi} + Q_{Pi}, \quad i = 1, 2 \tag{23}$$

Fig. 7 The modal shapes of FEM when $\alpha = 0$ and $\beta = 0$. **a** The 1st order modal shape. **b** The 2nd order modal shape. **c** The 3rd order modal shape. **d** The 4th order modal shape

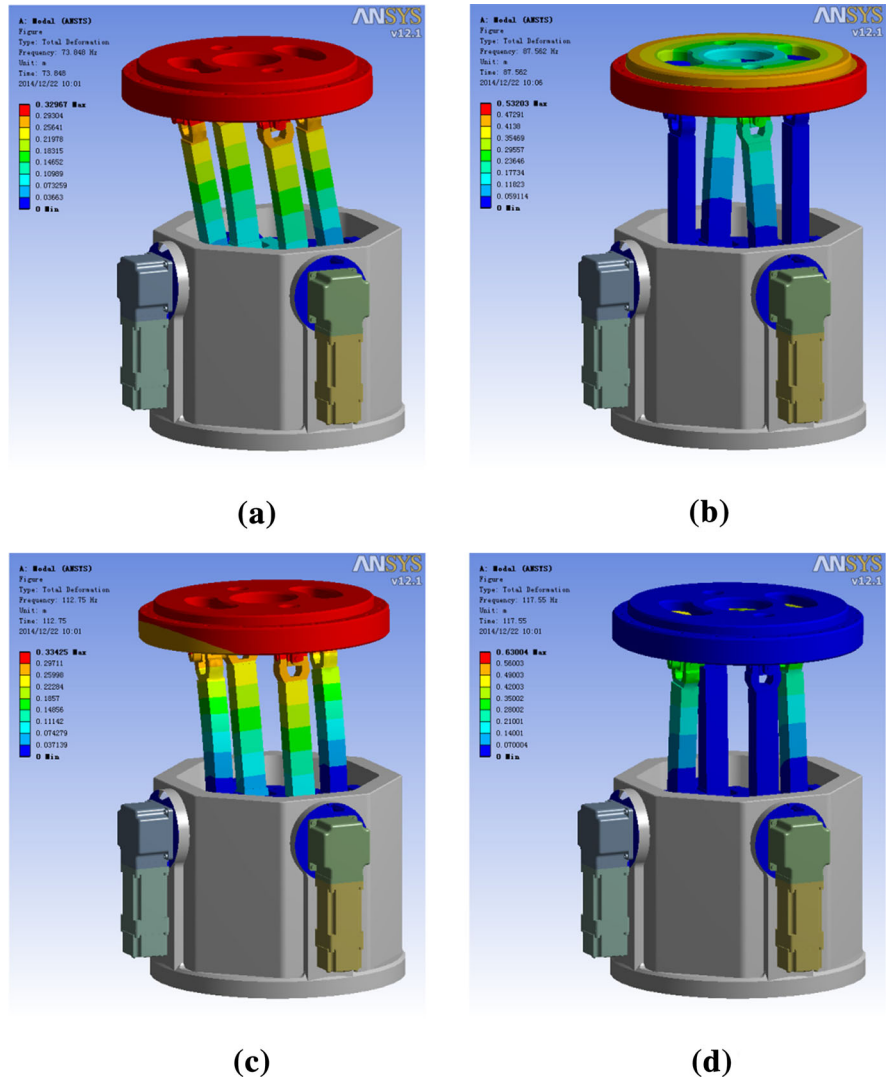


Table 2 The results of natural frequencies

Frequency	KED/Hz	FEM/Hz	Relative error (%)
1st	76.69	73.85	3.84
2nd	91.54	87.56	4.55
3rd	111.64	112.75	-0.98
4th	112.73	117.55	-4.10

where M_{Pi} , F_{Pi} , Q_{Pi} and U_{Pi} represent the mass matrix, the interactive force vector, the external force vector and the elastic deformation vector of the sub-plate I in the coordinate system $O - xyz$ for $i = 1$ and those of the sub-plate II for $i = 2$. It should be pointed out that

the elastic angles about w axis of the two sub-plates are different. In consequence, elastic deformations of point P are defined as $u_{Pi} = [\Delta x \ \Delta y \ \Delta z \ \Delta \alpha \ \Delta \beta \ \Delta \phi_i]^T$, where the elastic displacements are measured in the fixed coordinate system $O - xyz$ while the elastic angles are measured in the coordinate system $P - uvw$. Then Eq. (23) can be rewritten as follows.

$$M_{Pi}^e \ddot{u}_{Pi} = F_{Pi} + Q_{Pi}, \quad (i = 1, 2) \tag{24}$$

$$\text{where } M_{Pi}^e = M_{Pi} \begin{bmatrix} E_{3 \times 3} & 0_{3 \times 3} \\ 0_{3 \times 3} & R \end{bmatrix}.$$

The dynamic equation of the articulated travelling platform can be formulated as follows.

$$M_7 \ddot{U}_7 = F_7 + Q_7 \tag{25}$$

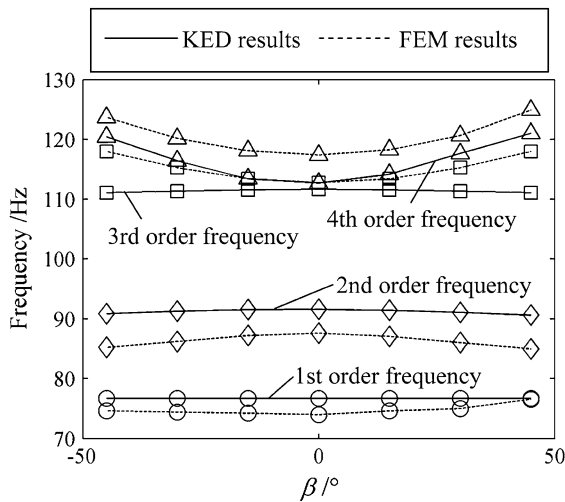


Fig. 8 The results comparison between KED and FEM when $\alpha = 0$

where

$U_7 = [\Delta x \ \Delta y \ \Delta z \ \Delta \alpha \ \Delta \beta \ \Delta \phi_1 \ \Delta \phi_2]^T$, M_7 , F_7 , Q_7 represent the mass matrix, the interactive force vector and the external force vector of the articulated travelling platform. Herein,

$$M_7 = \sum_{i=1}^2 J_{Pi}^T M_{Pi}^e J_{Pi}, \quad F_7 = \sum_{i=1}^2 J_{Pi}^T F_{Pi}, \quad Q_7 = \sum_{i=1}^2 J_{Pi}^T Q_{Pi}$$

where J_{Pi} is the mapping matrix between the general-ized coordinate vector of the plate and U_7 .

4.2 Deformation compatibility condition

The deformation compatibility condition is to set up the relations of generalized coordinates between different components. Considering the connection of adjacent components, deformation compatibility condition between the driven component and the articulated travelling platform can be formulated as follows.

$$\begin{bmatrix} U_{Ci13} \\ U_{Ci14} \\ U_{Ci15} \end{bmatrix} = \begin{bmatrix} E_{3 \times 3} & -S(a_i) \end{bmatrix} \times \begin{bmatrix} E_{3 \times 3} & 0_{3 \times 3} \\ 0_{3 \times 3} & R \end{bmatrix} u_{p1}, \quad (i = 1, 3) \tag{26}$$

$$\begin{bmatrix} U_{Ci13} \\ U_{Ci14} \\ U_{Ci15} \end{bmatrix} = \begin{bmatrix} E_{3 \times 3} & -S(a_i) \end{bmatrix} \times \begin{bmatrix} E_{3 \times 3} & 0_{3 \times 3} \\ 0_{3 \times 3} & R \end{bmatrix} u_{p2}, \quad (i = 2, 4) \tag{27}$$

where $a_i = Ra_{0i}$, $S(a_i) = \begin{bmatrix} 0 & -a_{iz} & a_{iy} \\ a_{iz} & 0 & -a_{ix} \\ -a_{iy} & a_{ix} & 0 \end{bmatrix}$.

Similarly, deformation compatibility condition between the driven component and the actuated component is expressed as follows.

$$\begin{bmatrix} U_{A26} \\ U_{A27} \\ U_{A28} \\ U_{A30} \\ U_{A31} \end{bmatrix} = \begin{bmatrix} U_{C11} \\ U_{C12} \\ U_{C13} \\ U_{C15} \\ U_{C16} \end{bmatrix}, \quad \begin{bmatrix} U_{A32} \\ U_{A33} \\ U_{A34} \\ U_{A36} \\ U_{A37} \end{bmatrix} = \begin{bmatrix} U_{C31} \\ U_{C32} \\ U_{C33} \\ U_{C35} \\ U_{C36} \end{bmatrix} \tag{28}$$

$$\begin{bmatrix} U_{B7} \\ U_{B8} \\ U_{B9} \\ U_{B10} \\ U_{B12} \end{bmatrix} = \begin{bmatrix} U_{C21} \\ U_{C22} \\ U_{C23} \\ U_{C24} \\ U_{C26} \end{bmatrix}, \quad \begin{bmatrix} U_{B26} \\ U_{B27} \\ U_{B28} \\ U_{B29} \\ U_{B31} \end{bmatrix} = \begin{bmatrix} U_{C41} \\ U_{C42} \\ U_{C43} \\ U_{C44} \\ U_{C46} \end{bmatrix} \tag{29}$$

4.3 Elasto-dynamic equations

The elasto-dynamic equation of the novel 2-DoF RPM can be calculated by elasto-dynamic models of components with the deformation compatibility conditions as

$$M_s \ddot{u} + K_s U = F_s \tag{30}$$

where U denotes the generalized coordinate vector of the 2-DoF RPM which contains 121 elements. Generalized coordinate vector of the whole mechanism and individual components has the following relation,

$$U_j = B_j U \quad (j = 1 \sim 7)$$

where B_j denotes the coordinate harmonized matrix of the components in the fixed coordinate system. M_s , K_s represent the mass matrix and the stiffness matrix of the novel 2-DoF RPM. F_s denotes the generalized external force. Herein,

$$M_s = \sum B_j^T M_j B_j, \quad K_s = \sum B_j^T K_j B_j$$

$$F_s = \sum B_j^T F_j B_j$$

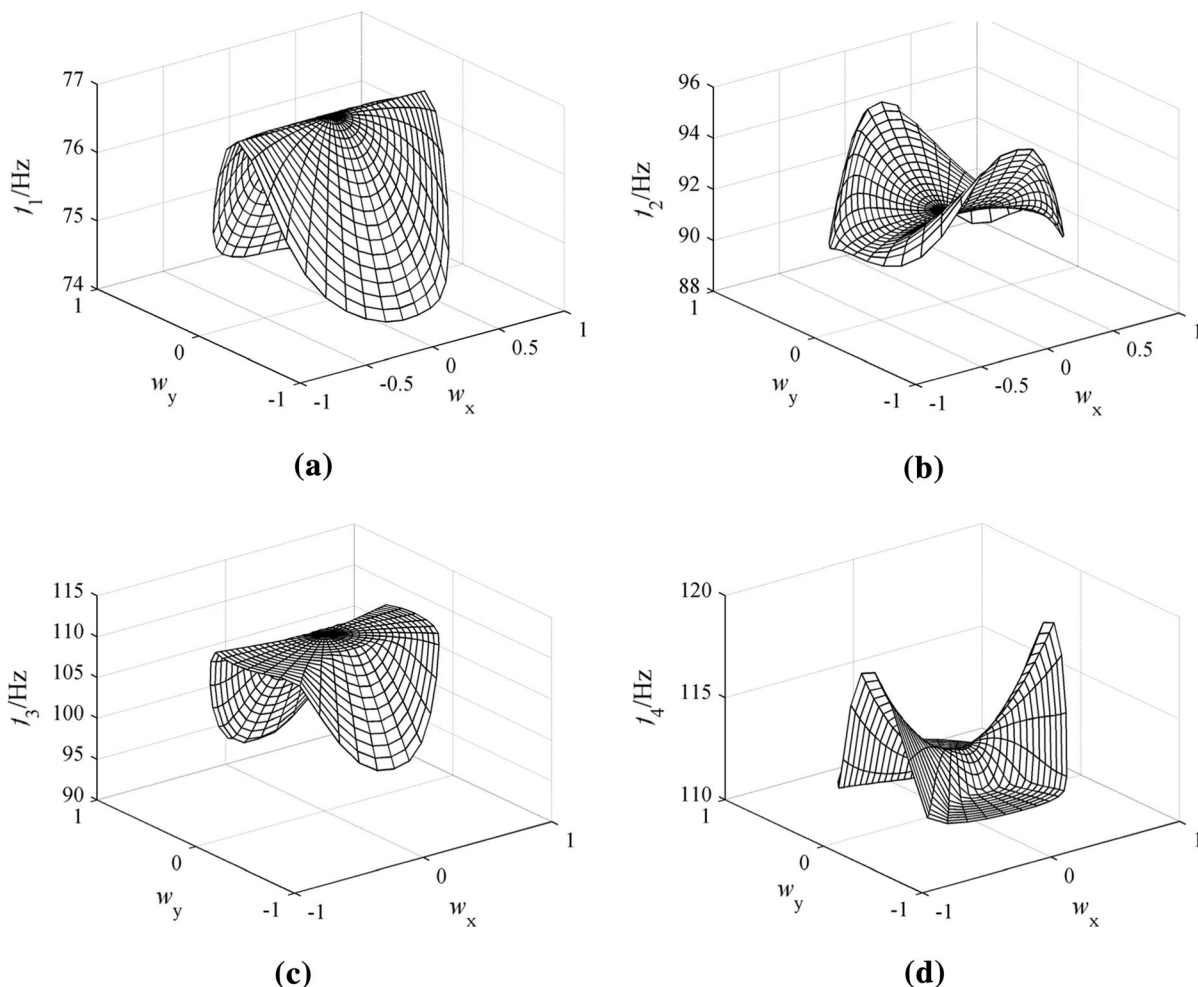


Fig. 9 The distributions of frequencies. **a** The 1st order natural frequency. **b** The 2nd order natural frequency. **c** The 3rd order natural frequency. **d** The 4th order natural frequency

The undamped free vibration equation of the novel 2-DoF RPM can be derived from Eq. (30) as

$$\mathbf{M}_s \ddot{\mathbf{u}} + \mathbf{K}_s \mathbf{U} = 0 \quad (31)$$

Then the natural frequencies are calculated through

$$\det(\mathbf{K}_s - \omega^2 \mathbf{M}_s) = 0 \quad (32)$$

5 Example and discussion

Under the guidance of the analysis flow in Sect. 4, an example is given to illustrate the natural frequencies of the novel 2-DoF RPM with the parameters shown in Table 1. As shown in Fig. 7, to verified the theoretical

method, simulation conducted by Ansys Workbench software [19] is applied when $\alpha = 0$, $\beta = 0$. The comparisons between the two approaches are illustrated in Table 2 and Fig. 8. It is obvious that the natural frequencies obtained by KED method are similar to those by finite element software, which may be resulted from the difference of finite element models and the real components with irregular shape and dimension. And the errors are within 5 %, indicating good consistency of the two methods and validating the effectiveness of KED method.

After verified the theoretical method, distributions of natural frequencies in the prescribed workspace are demonstrated analytically in Fig. 9. w_x and w_y are used to represent the projection of the unit vector \mathbf{w} on the x axis and that on the y axis. As shown in Fig. 9, 1st,

2nd, 3rd, 4th natural frequencies are all plane symmetrical about $w_y = 0$ and approximately symmetrical about plane $w_x = 0$. For the 1st and 3rd natural frequencies, they decrease as the w_y goes up while they remain constant as the change of w_x . The variations of 2nd and 4th natural frequencies are opposite to each other. 2nd natural frequency gradually goes up with the increase of w_y but drops when w_x becomes bigger. On the contrary, 4th natural frequency slowly decreases as the increment of w_y while it dramatically rises as w_x climbs up.

6 Conclusions

Concerning the application for pose-adjusting module of 5-DoF hybrid machining centre, this paper proposed a novel 2-DoF RPM and carried out its elasto-dynamic analysis. The following conclusions can be drawn:

- (1) By introducing an articulated travelling platform, high rotational capability without parasitic motion is achieved by the novel 2-DoF RPM which possess advantages in terms of high rigidity, compact structure and good dynamic performance.
- (2) By utilizing the KED method, the elasto-dynamic model of the novel 2-DoF RPM can be assembled by those of components in the light of deformation compatibility condition.
- (3) The natural frequencies of the novel 2-DoF RPM are calculated and verified by finite element software. The result shows that the novel 2-DoF parallel mechanism is of good elasto-dynamic performance.

Acknowledgments This research work was supported by the National Natural Science Foundation of China (Grant No. 51205278, 51475321), Ph.D. Programs Foundation of Ministry of Education of China (Grant No. 2012003211003, 2012003212003), and Tianjin Research Program of Application Foundation and Advanced Technology (Grant No. 13JCQNJC04600).

References

1. Li YG, Liu HT, Zhao XM, Huang T, Chetwynd DG (2010) Design of a 3-DOF PKM module for large structural component machining. *Mech Mach Theory* 45(6):941–954
2. Neumann KE (2002) Tricept applications. In: Proceedings of the 3rd Chemnitz parallel kinematics seminar, Zwickau, Germany, pp 547–551
3. Bruno S (1999) The Tricept robot: inverse kinematics, manipulability analysis and closed-loop direct kinematics algorithm. *Robotica* 17(4):437–445
4. Sun T, Song YM, Li YG, Zhang J (2010) Workspace decomposition based dimensional synthesis of a novel hybrid reconfigurable robot. *ASME J Mech Robot* 2(3):031009
5. Song YM, Lian BB, Sun T, Dong G, Qi Y (2014) A novel 5-DoF fully parallel manipulator and its kinematic optimization. *ASME J Mech Robot* 6(4):041008
6. Palpacelli M, Palmieri G, Carbonari L, Callegari M (2014) Experimental identification of the static model of the HPKM Tricept industrial robot. *Adv Robot* 28(19):1291–1304
7. Kong XW (2011) Forward displacement analysis and singularity analysis of a special 2-DOF 5R spherical parallel manipulator. *ASME J Mech Robot* 3(2):024501
8. Wu C, Liu XJ, Wang LP, Wang JS (2010) Optimal design of spherical 5R parallel manipulators considering the motion/force transmissibility. *ASME J Mech Des* 132(3):031002
9. Wu C, Liu XJ, Wang JS (2009) Force transmission analysis of spherical 5R parallel manipulators. In: Proceedings of the international conference on reconfigurable mechanisms and robots, London, England: 331–336
10. Baumann R, Maeder W, Glauser D (1997) The PantoScope: a spherical remote-center-of-motion parallel manipulator for force reflection. In: Proceedings of the 1997 IEEE international conference on robotics and automation, Albuquerque, New Mexico
11. Gosselin C, Caron F (1999) Two degree-of-freedom spherical orienting device. US Patent 5,966,991
12. Rosheim ME, Sauter GF (2002) New high-angulation omnidirectional sensor mount. In: International symposium on optical science and technology. International society for optics and photonics, pp 163–174
13. Sofka J, Skormin V, Nikulin V, Nicholson DJ (2006) Omni-Wrist III—a new generation of pointing devices. Part I. Laser beam steering devices—mathematical modeling. *IEEE T Aero Elec Sys* 42(2):718–725
14. Chen B, Zong GH, Yu JJ, Dong X (2013) Dynamic modeling and analysis of 2-DOF quasi-sphere parallel platform. *Chin J Mech Eng-En* 49(13):24–31
15. Liu XJ, Wang JS, Xie FG (2008) A decoupled parallel spindle structure. CN Patent 101,269,465
16. Song YM, Dong G, Sun T, Zhao XM, Wang PF (2012) A novel parallel mechanism with two rotational degrees-of-freedom. CN Patent 2,012,105,131,575
17. Zhang C, Huang YQ, Wang ZL, Chen SX (1997) Analysis and design of the elastic linkages, 2nd edn. China Machine Press, Beijing
18. Bhatti MA (2005) Fundamental finite element analysis and applications. Wiley, Canada
19. Palmieri G, Martarelli M, Palpacelli MC, Carbonari L (2014) Configuration-dependent modal analysis of a cartesian parallel kinematics manipulator: numerical modeling and experimental validation. *Meccanica* 49(4):961–972